Available online at www.sciencedirect.com
ScienceDirect
Journal of Power Sources 166 (2007) 244–249
JOURNAL OF POWER SOURCES
www.elsevier.com/locate/jpowsour

Short communication

Cathodic performance of (V_2O_5 + PEG) nanobelts for Li ion rechargeable battery

Ch.V. Subba Reddy [a,b], J. Wei [a], Z. Quan-Yao [a], D. Zhi-Rong [a], Chen Wen [a,1], Sun-il Mho [b], Rajamohan R. Kalluru [c,*]

[a] *Institute of Materials Science and Engineering, Wuhan University of Technology, Wuhan 430070, PR China*
[b] *Division of Energy Systems Research, Ajou University, Suwon 443-749, Republic of Korea*
[c] *Mississippi Ethanol LLC, 86 Industrial Park Boulevard, Winona, MS 38967-186, USA*

Received 5 December 2006; received in revised form 23 December 2006; accepted 2 January 2007
Available online 14 January 2007

Abstract

Vanadium Oxide (V_2O_5) nanobelts were synthesized, intercalating with a conducting polymer polyethylene glycol (PEG), by simple hydrothermal process. Investigations were conducted by X-ray diffractometry (XRD), Fourier transform infrared spectroscopy (FTIR), Differential scanning calorimetry (DSC) and Scanning electron microscopy (SEM) and Cyclic voltammetry (CV). The results show that the H atoms in PEG are hydrogen bonded with the O atoms of the V=O bonds of the V_2O_5, which effectively shielded against electrostatic interaction between the V_2O_5 interlayer and Li^+ ions when the V_2O_5 is modified by the intercalation of PEG. The broad endothermic peak temperature increases with increasing concentration of PEG content in V_2O_5 nanobelts. Cathodic performance of $PEG_xV_2O_5$ ($x = 0$, 0.5 and 1) nanobelts for Li ion rechargeable battery was investigated. The V_2O_5 nanobelts exhibit a high specific discharge capacity of 397.61 mAh g^{-1} for Li ion electrochemical intercalation.

Keywords: Nanobelts; Polyethyleneglycol; V_2O_5 Xerogel; Li-battery

1. Introduction

Recent years have seen a dramatic proliferation in portable electronic devices. Lithium ion rechargeable batteries are now widely used as power source for mobile electronic systems such as mobile phones, camcorders, laptops and personal digital-assistants (PDAs). Presently, transition metal oxides containing Li such as $LiNiO_2$, $LiMn_2O_4$ and mostly $LiCoO_2$ are used for cathodes in rechargeable batteries. However, owing to the fact that Co is a scarce material, an alternative cathode material for $LiCoO_2$ is now strongly required. Currently, $LiMn_2O_4$ or Mn based oxides are expected to be the most promising alternative cathode materials. However, degradation in capacity at higher temperatures causes a problem when Mn based oxide cathode is used in a Li ion rechargeable battery. Therefore, development of alternative new cathode material is essential for improved performance of the Li ion rechargeable battery.

Vanadium oxide and derived compounds are receiving significant focus as a cathode material for Li ion batteries [1–3] owing to their structure and properties. While vanadium oxide phase containing mixed valance vanadium (V^{5+} and V^{4+}) crystallizes in 3D network structures, it can be regarded as a layered structure in which VO_5 square pyramids are connected by shared corners and edges [4]. This structural peculiarity permits the synthesis of $M_xV_2O_5$ phase with various polymer ions embedded between the layers without far-reaching restructuring. Over the past few years, mesoporous sieves of vanadium oxide have been synthesized via the intercalation of various polymers [5,6].

Off late, much attention has been drawn to one-dimensional (1D) nanostrctured materials, such as nanowires, nanobelts, nanotubes and nanorods, because of fundamental research importance and their wide ranging potential applications in nanodevices [7]. Semiconducting 1D nanomaterials are known to have many interesting physical properties and great applications in electrochemical devices, for example, nanobelts ethanol-sensing devices with excellent potential for sensor applications

* Corresponding author. Tel.: +1 6623258444; fax: +1 6623258465.
E-mail addresses: chenw@mail.whut.edu.cn (C. Wen), rkalluru@icet.msstate.edu (R.R. Kalluru).
[1] Tel.: +86 27 878651107; fax: + 86 27 87864580.

0378-7753/$ – see front matter © 2007 Elsevier B.V. All rights reserved.
doi:10.1016/j.jpowsour.2007.01.010

[8]. Therefore, synthesis of novel nanobelts is very important to meet more stringent application requirements.

Many researchers had modified V_2O_5 xerogels with polymer such as poly (vinyl pyrrolidone) (PVP), polyaniline (PANI), poly (ethylene oxide) (PEO) and polypyrrole [9–11] in thin film technology. A few studies are available on polymer template using nanometerial synthesis. Generally, to obtain nanobelts from V_2O_5 xerogel takes 14 days of hydrothermal reaction time with out template. By using polymer template the hydrothermal reaction time decreased from 14 to 7 days and also the amounts of the products in gram quantities could be obtained in high yield without the requirement of delicate equipment. The yield of the PEGxV_2O_5 nanobelts was estimated to be 70–80% from different batches of synthesis, and has been verified by SEM. But there is a limitation, i.e., less specific discharge capacity for polymer intercalated V_2O_5 nanobelts due to decrease of average oxidation state of vanadium. This problem can be rectified by post-treating oxygen or aging polymer and V_2O_5 solution for a long time. Present paper reports the synthesis and characterization of $PEG_xV_2O_5$ ($x = 0$, 0.5 and 1) nanobelts.

2. Experimental

2.1. Synthesis of $PEG_xV_2O_5$ ($x = 0$, 0.5 and 1) nanobelts

The V_2O_5 xerogel was synthesized according to the method described by Chen and co-workers [9]. Polyethylene glycol (PEG) (MW = 10,000 g mol^{-1}) solution, obtained form Aldrich, was mixed with the V_2O_5 solution to form a mixed sol. The molar ratio of PEG to V_2O_5 was x:1 ($x = 0$, 0.5, and 1). The mixed solutions were stirred for 24 h at room temperature and then poured into Teflon-lined autoclaves and kept at 180 °C for 7 days in a hot oven. After the hydrothermal reaction, the obtained products in light green color were washed with distilled water and dried at 100 °C for 24 h.

2.2. Characterization

The products were characterized using a HZG4/B-PC X-ray diffractrometer with Co Kα radiation and graphite monochrometer. FTIR absorption spectra of the films were recorded using a 60-SXB IR spectrometer with a resolution of 4 cm^{-1}. The measurements were taken over a wave number range of 400–4000 cm^{-1}. Raman spectra were taken under ambient condition by using a Renishaw in Via Raman microscope excited with a 514-nm Ar^+ laser. The size and morphology of the $PEG_xV_2O_5$ ($x = 0$, 0.5, and 1) nanobelts were determined using the JSM-5610LV scanning electron microscope. For the DSC measurements a Netzsch STA 409 PC, operating in dynamic mode (heating rate = 10 K min^{-1}), was employed. Samples of ≈5 mg samples were placed in sealed aluminium pans for the measurements. Prior to using the calorimeter, the system was calibrated to metal standards, an empty aluminium pan being used as a reference.

The cyclic voltammogram (CV) was performed by electrochemical method in a non-aqueous lithium cell using 1 M $LiClO_4$ dissolved in propylene carbonate (PC) electrolyte. The electrochemical cell was a standard three-electrode system. Indium tin oxide (ITO) conducting glass coated with the modified V_2O_5 xerogel film and platinum foil were used as working electrode and counter electrode, and standard calomel electrode was used as a reference electrode.

The electrochemical characteristics were estimated out using a multichannel galvanostat/potentiostat system (MacPile). Electrochemical cells were prepared using a lithium pellet as negative electrode, a 1 mol dm^{-3} solution of $LiPF_6$ in ethylene carbonate (EC)/dimethyl carbonate (DMC) as electrolyte and a pellet made of $PEG_xV_2O_5$ ($x = 0$, 0.5 and 1) nanobelts, acetylene black and PTFE in a 75:20:05 ratio as positive electrode. The amount of active material loaded in the experiment was 11.46 mg. The electrodes were dried at 100 °C in a vacuum furnace for 24 h before used to remove/minimize the water content in the material.

3. Results and discussion

3.1. XRD analysis

Fig. 1 shows the XRD patterns for the $PEG_xV_2O_5$ ($x = 0$, 0.5, and 1) nanobelts. All diffraction peaks were well indexed to show that system is a tetragonal one with the lattice constants $a = 14.259$, $b = 14.259$, $c = 12.576$ and $\alpha = \beta = \gamma = 90°$ (JCPDS No. 00-045-1074). The diffraction peaks of the polyethylene glycol intercalated $PEG_xV_2O_5$ ($x = 0.5$ and 1) remain unchanged, indicating that the original structure is retained.

3.2. IR analysis

Fig. 2 shows the FTIR spectrum of the as-prepared $PEG_xV_2O_5$ ($x = 0$, 0.5, and 1) nanobelts. The absorption bands at 524 and 852 cm^{-1} are respectively assigned as V–O–V deformation. The peak at 1023 cm^{-1} is characteristic of the stretching vibration of the terminal vanadyl, V=O [12]. The peak at 3451 cm^{-1} is attributed to the O–H stretching vibration of H_2O. We found that both the V–O–V deformation and

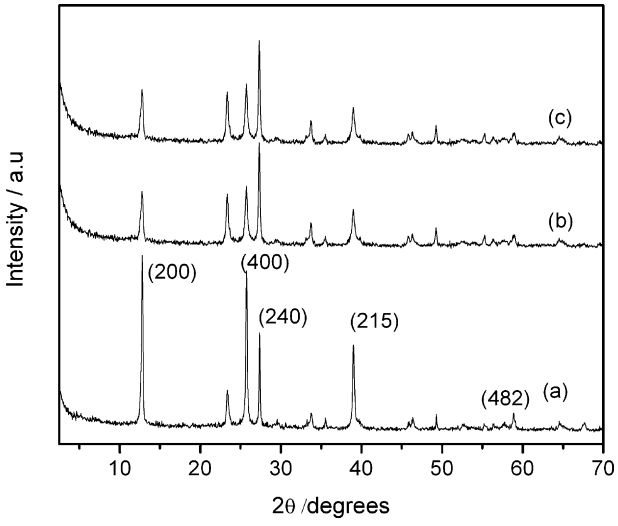

Fig. 1. XRD spectra of (a) V_2O_5, (b) PEG $_{0.5}$ V_2O_5, and (c) PEG_1 V_2O_5 nanobelts.

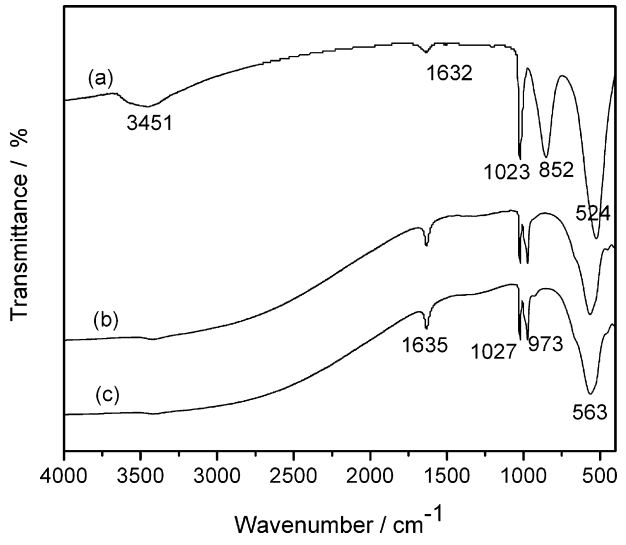

Fig. 2. FTIR spectra of (a) V_2O_5, (b) PEG $_{0.5}$ V_2O_5, and (c) PEG_1 V_2O_5 nanobelts.

the stretching vibration of the terminal vanadyl, V=O modes shift towards higher wavenumber in the $PEG_xV_2O_5$ ($x = 0$, 0.5, and 1) nanobelts. The V=O mode shifts from 1023 to 1027 cm^{-1} in $PEG_xV_2O_5$ ($x = 1$), which indicates that the V=O···H bond is formed in the nanocomposite materials [13]. Strong interaction between the vanadyl group and the incorporated polymer has been proved by the shifts of the vanadyl vibration peaks which are evidenced to the polymer intercalation in V_2O_5 layers under hydrothermal condition.

3.3. Raman spectra analysis

Raman spectrum of V_2O_5 nanobelts is shown in Fig. 3. The known V–O–V stretching modes are observed at 400, 478 and 523 cm^{-1}, while other bands below 400 cm^{-1} can be assigned to V–O and V–O–V bending modes [14,15]. The band at 996 cm^{-1} is assigned to V=O stretching of distorted octahedral and distorted square pyramids, while the band at 702 cm^{-1} is due to coordination of vanadium atoms with the three oxygen atoms.

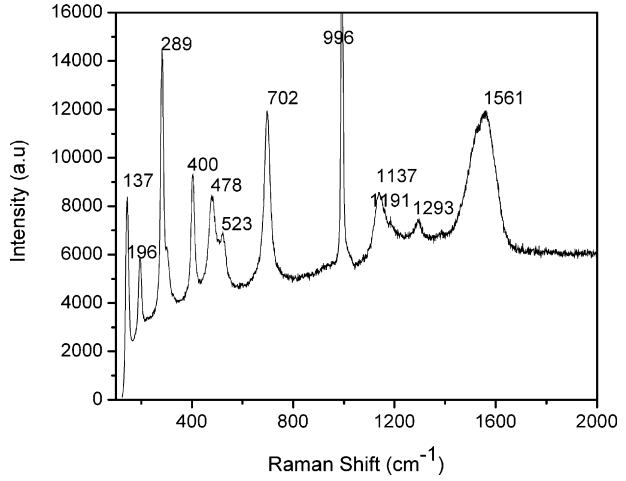

Fig. 3. Raman spectra of V_2O_5 nanobelts.

The position and relative intensity of the Raman peaks are in good agreement with that reported for V_2O_5 [16].

3.4. Morphology examination

The morphology of as-prepared products was observed using SEM images. Fig. 4 show that the nanobelts have rectangle shape with relatively uniform widths of 100–500 nm and thickness of 40–80 nm along their entire length.

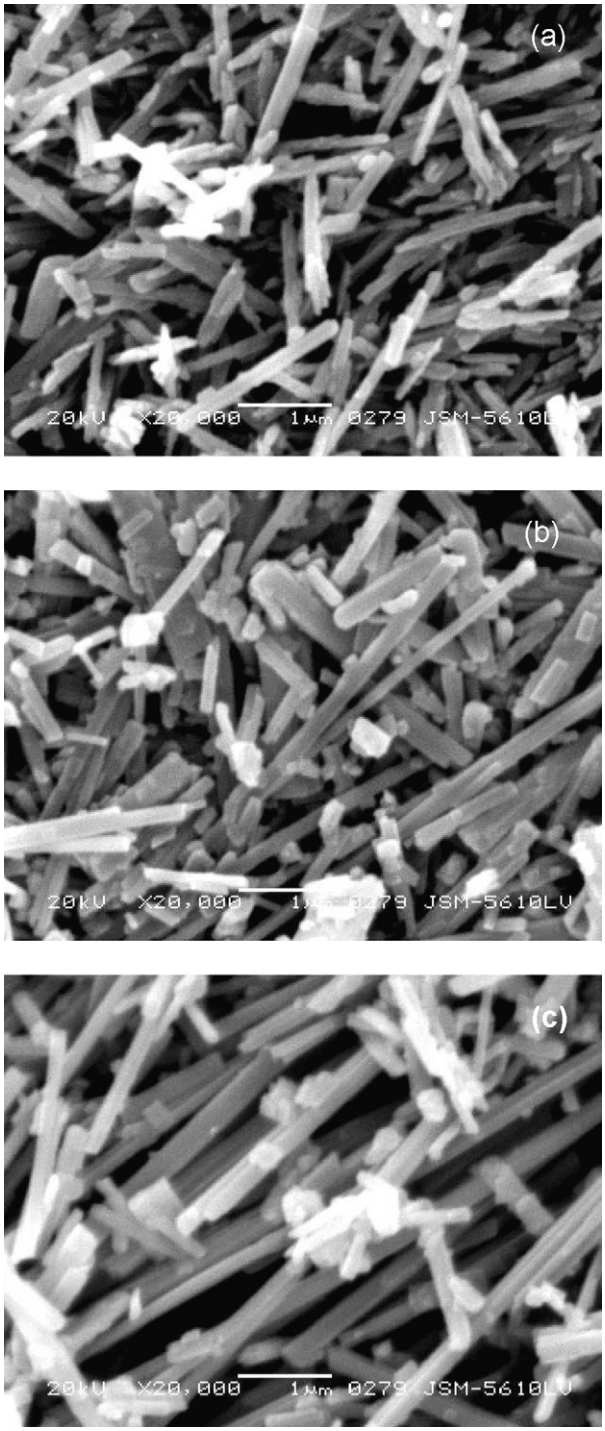

Fig. 4. SEM photographs of (a) V_2O_5, (b) PEG $_{0.5}$ V_2O_5, and (c) PEG_1 V_2O_5 nanobelts.

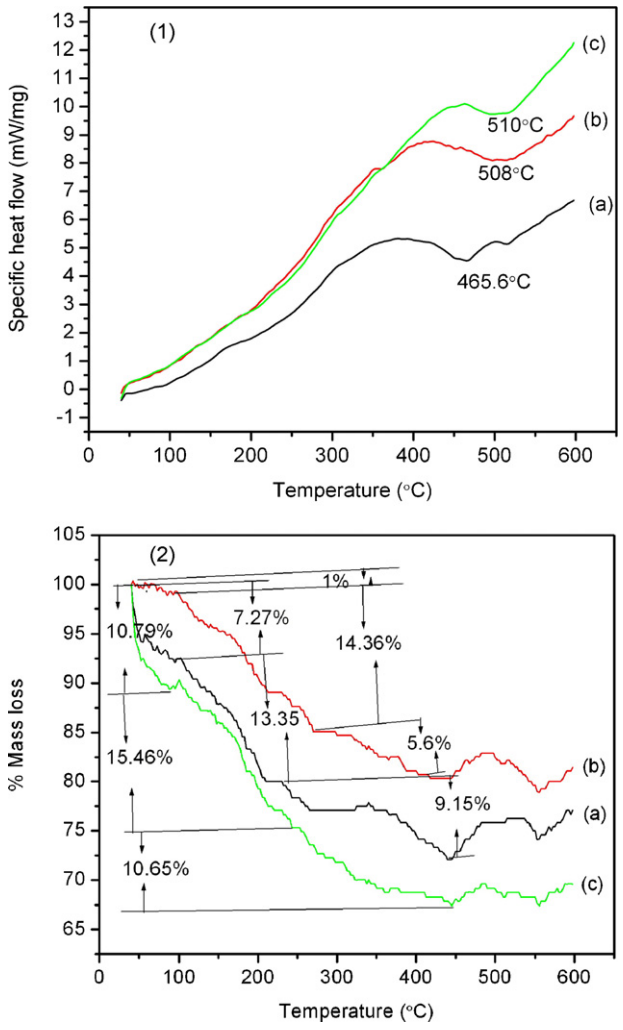

Fig. 5. (1) DSC curves of (a) V_2O_5, (b) PEG $_{0.5}$ V_2O_5, and (c) PEG_1 V_2O_5 nanobelts. (2) TG plots of (a) V_2O_5, (b) PEG $_{0.5}$ V_2O_5, and (c) PEG_1 V_2O_5 nanobelts. Estimated % of water loss is shown with temperature.

3.5. Thermal analysis

DSC results show that there was a single broad endothermic peak corresponding to the combustion of the polymer in the region 500–520 °C (Fig. 5(1)) for $PEG_xV_2O_5$ ($x = 0.5$ and 1) nanobelts. In the case of V_2O_5 nanobelts, two endothermic peaks were observed. The broad endothermic peak temperature was increased with polymer concentration in V_2O_5, which could be the responsible for the variation of the conductivity and electrochemical properties of the $PEG_xV_2O_5$ ($x = 0.5$ and 1) cathodes.

The thermal stability of the $PEG_xV_2O_5$ ($x = 0$, 0.5, and 1) nanobelts in nitrogen was examined by thermogravimetry analysis (TGA) experiment. All samples show a continuous weight loss up to 260 °C (Fig. 5(2)) due to the loss of weakly bound water. The second wave of weight loss extends up to around 350 °C, due to the release of the intramolecular water and the water molecules bound to vanadium. The amount of water loss was estimated from TGA curves and shown Fig. 5(2). V_2O_5 compounds have 'bidimensional' structure, which is stabilized by interlayer water molecules. The replacement of water molecules by hydrophobic polymer chains differs from one composition to another composition. The amount of water in the cathode material varies in the following order PEG (0.5) $V_2O_5 < V_20_5 < PEG(1.0)V_2O_5$.

3.6. CV analysis

The electrochemical performance and reversibility of the $PEG_xV_2O_5$ ($x = 0$, 0.5, and 1) films were tested by the cyclic

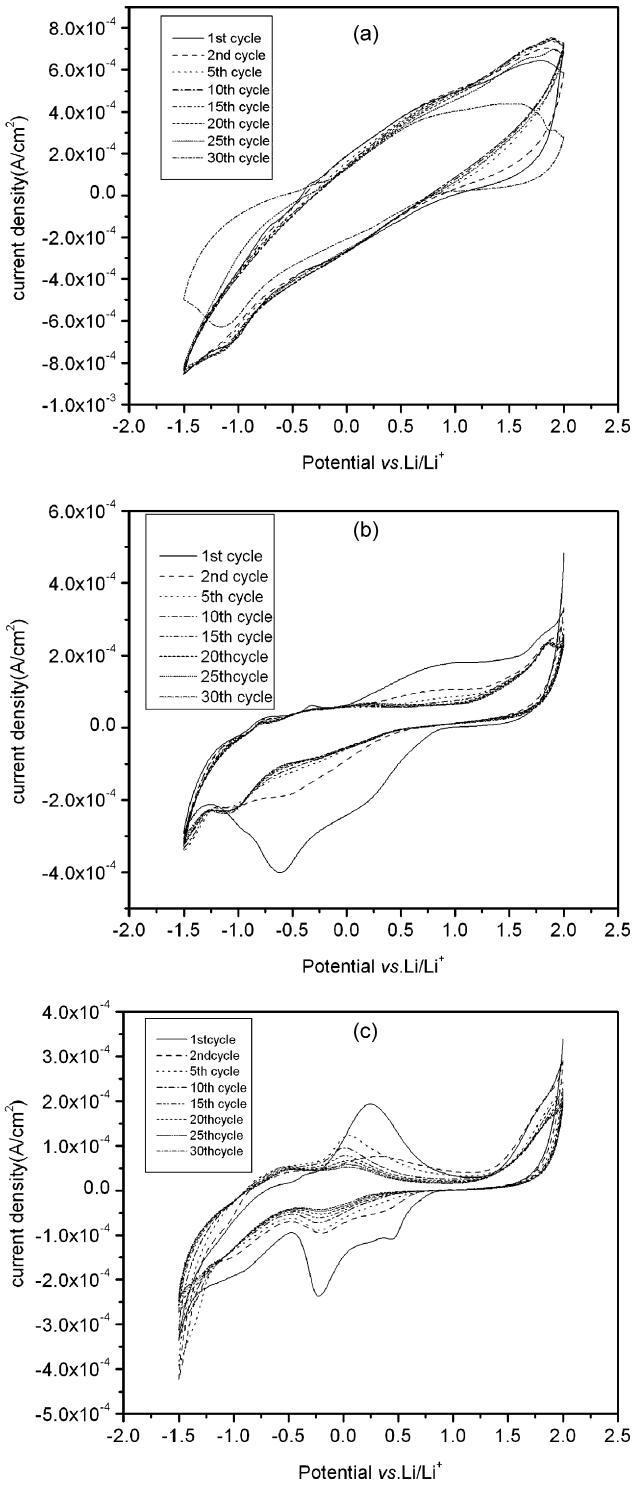

Fig. 6. CV curves of (a) V_2O_5, (b) PEG $_{0.5}$ V_2O_5, and (c) PEG_1 V_2O_5.

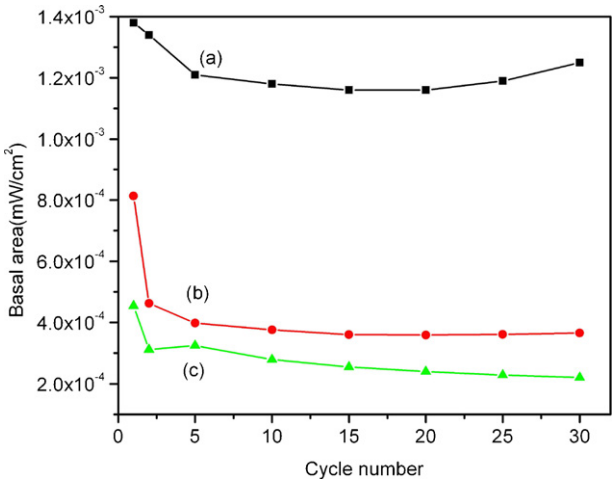

Fig. 7. Basal area curves of (a) V_2O_5, (b) PEG $_{0.5}$ V_2O_5, and (c) PEG_1 V_2O_5.

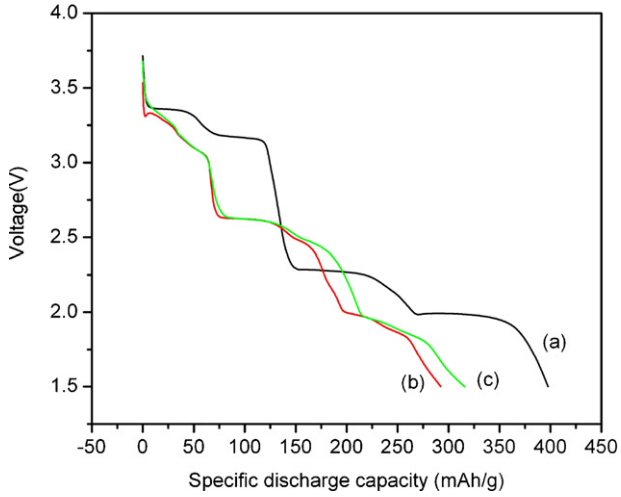

Fig. 8. First discharge curves of (a) V_2O_5, (b) PEG $_{0.5}$ V_2O_5, and (c) PEG_1 V_2O_5 nanobelts battery.

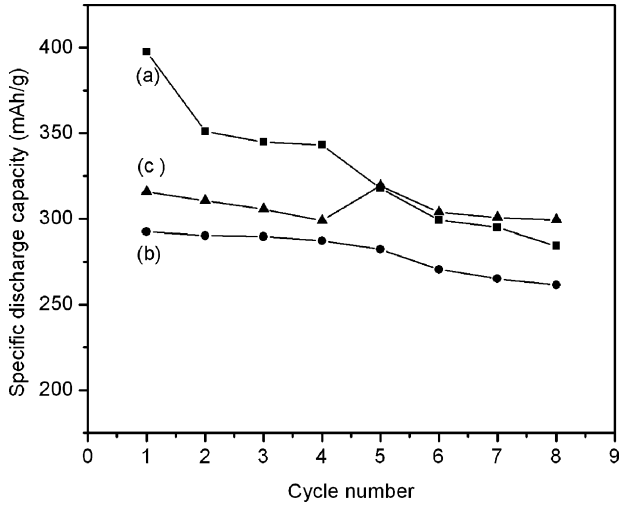

Fig. 9. Cycling property of (a) V_2O_5, (b) PEG $_{0.5}$ V_2O_5, and (c) PEG_1 V_2O_5 nanobelts battery.

voltammogram (CV). The area A_i (i is the number of cycles) that was enclosed by each cycle represents the amount of insertion of Li^+ ions. The cycle efficiency was calculated using the following formula,

$$Q_i = \frac{A_i}{A_1}$$

where Q_i is the cycle efficiency, A_1 the area of the first curve and A_i is the area the ith cycle curve. Fig. 6 shows cyclic voltammograms of the $PEG_xV_2O_5$ ($x = 0$, 0.5, and 1) films, respectively, in which the first, second, fifth, 10th, 15th, 20th, 25th and 30th cycle curves are shown. The peak potentials shift considerably with cycling, and the amount of the insertion of Li^+ ions decreases. Fig. 7 shows plots of the basal area versus cycle number for $PEG_xV_2O_5$ ($x = 0$, 0.5, and 1) films. The voltammetry for the three materials was different with different redox and oxidation peak voltages. The composite also shows a narrow cyclic voltammetric curve and lowered charging current at positive potential of the peak. The characteristic of the redox response is due to the decreased average vanadium oxidation state with the intercalation of polymers towards lithium insertion [10]. This is evidenced that the basal area at the second cycle A_2 for the $PEG_xV_2O_5$ ($x = 0.5$ and 1) is 468 and 314 $\mu W\,cm^{-2}$, and for V_2O_5 is 1988 $\mu W\,cm^{-2}$. These results affect battery performance of the PEG$_x$V2O5 ($x = 0.5$ and 1) nanobelts.

3.7. Electrochemical characteristics

The initial discharge curves of $PEG_xV_2O_5$ ($x = 0$, 0.5, and 1) nanobelts batteries are shown in Fig. 8. The discharge capacitance of the $PEG_xV_2O_5$ ($x = 0.5$ and 1) nanobelts batteries are lower than that of the V_2O_5 nanobelts battery. The measured discharge capacitance of the as-prepared V_2O_5 nanobelts was 398 mAh g^{-1} in the potential range from 3.75 to 1.5 V and 292, 317 mAh g^{-1} for the $PEG_xV_2O_5$ ($x = 0.5$ and 1) nanobelts batteries, respectively. Fig. 9 shows eight complete charge–discharge cycles of the battery. The specific discharge capacity is 284 mAh g^{-1} after eight cycles of the V_2O_5 nanobelts and the cell exhibits a capacity loss of only 29%, which indicates that it has good cycle stability. The specific discharge capacity is 261 mAh g^{-1} after eight cycles of the $PEG_xV_2O_5$ ($x = 0.5$) battery and it exhibits a capacity loss of 11%. The specific discharge capacity is 299 mAh g^{-1} after eight cycles of the $PEG_xV_2O_5$ ($x = 1$) battery and it exhibits a capacity loss of 6%, which indicates that it has more economical electrochemical performance. An improved discharge capacity and cycle stability of the PEGxV$_2$O$_5$ ($x = 0.5$ and 1) batteries are expected with the oxygen post treatment for the $PEG_xV_2O_5$ ($x = 0.5$ and 1) nanobelts.

4. Conclusions

$PEG_xV_2O_5$ ($x = 0$, 0.5 and 1) nanobelts were prepared successfully by using hydrothermal treatment method with no catalysts. Polyethylene glycol has been intercalated into V_2O_5 xerogel. The intercalation was confirmed by XRD, FTIR and Raman spectroscopy. The electrochemical measurements show

that V_2O_5 nanobelts have high specific charge capacity than the $PEG_xV_2O_5$ ($x = 0.5$ and 1) nanobelts.

Acknowledgements

One of the authors (CVSR) thank the Wuhan University of Technology for his Post Doctoral Fellowship. Opening Foundation of Hubei Ferroelectric and Piezoelectric Materials and Devices Key Laboratory supported this work.

References

[1] J.M. Tarascon, M.A. Armand, Nature 414 (2001) 359.
[2] M.E. Spahr, P.S. Bitterli, R. Nesper, O. Haas, P. Novak, J. Electrochem. Soc. 146 (1999) 2780.
[3] J.S. Btaithwaite, C.R.A. Catlow, J.D. Gale, J.H. Harding, Chem. Mater. 11 (1999) 1990.
[4] H.G. Bachmann, F.R. Ahmed, W.H. Bames, Z. Kristallogr, 15 (1961) 110.
[5] J. Glay, J. Solid State Chem. 100 (1992) 229.
[6] V. Luca, J.M. Hook, Chem. Mater. 9 (1997) 2731.
[7] A.P. Alivisatos, Science 271 (1996) 933.
[8] X. Wu, Y. Tao, L. Dong, J. Hong, J. Mater. Chem. 14 (2004) 901.
[9] Ch.V. Subba Reddy, X. Han, A.P. Jin, Q.Y. Zhu, L.Q. Mai, W. Chen, Electrochem. Commun. 8 (2006) 279.
[10] N.G. Park, K.S. Ryu, Y.J. Park, M.G. Kang, D.K. Kim, S.G. Kang, K.M. Kim, S.H. Chang, J. Power Sources 103 (2002) 273.
[11] G.R. Goward, F. Leroux, L.F. Nazar, Electrochim. Acta 43 (1998) 1307.
[12] S. Webster, R. Czerw, R. Nesper, J. DiMaio, J.F. Xu, J. Ballato, D.L. Carroll, J. Nanosci. Nanotech. 4 (2004) 260.
[13] J. Harreld, H.P. Wong, B.C. Dave, F. Leroux, B. Dunn, L.F. Nazar, J. Non-Cryst. Solids 225 (1998) 319.
[14] F.D. Hardeastle, I.E. Wach, J. Phys. Chem. 95 (1991) 5031.
[15] S. Onodera, Y. Ikegami, Inorg. Chem. 19 (1980) 615.
[16] V.V. Fomichev, P.I. Ukrainskaya, T.M. Ilyin, Spectrochim. Acta A53 (1997) 195.